Rapid-Update Radar Observations of Z_{DR} Column Depth and Its Use in the Warning Decision Process

CHARLES M. KUSTER,[a,b,c] JEFFREY C. SNYDER,[b] TERRY J. SCHUUR,[a,b,c] T. TODD LINDLEY,[d] PAMELA L. HEINSELMAN,[b,e] JASON C. FURTADO,[e] JEFF W. BROGDEN,[a,b,c] AND ROBERT TOOMEY[a,b,c]

[a] *Cooperative Institute for Mesoscale Meteorological Studies, Norman, Oklahoma*
[b] *NOAA/OAR/National Severe Storms Laboratory, Norman, Oklahoma*
[c] *University of Oklahoma, Norman, Oklahoma*
[d] *NOAA/National Weather Service, Norman, Oklahoma*
[e] *School of Meteorology, University of Oklahoma, Norman, Oklahoma*

(Manuscript received 4 February 2019, in final form 3 June 2019)

ABSTRACT

The recent dual-polarization upgrade to the National Weather Service radar network provides forecasters with new information to use during operations, yet currently this information is not routinely used to explicitly make warning decisions. One potential way to increase operational use is to link new radar signatures and products to existing forecaster conceptual models and the warning decision process. Over the past several years, a unique dataset consisting of rapid-update (<2-min volumes) radar data of storms over central Oklahoma has been collected to examine possible links between Z_{DR} columns and forecaster conceptual models. In total, over 1400 volume scans from 42 storms—ranging from tornadic supercells to nonsevere multicells—are used to relate Z_{DR} column depth to storm reports and radar signatures typically used to issue warnings, such as −20°C reflectivity core and low-level mesocyclone evolution. After completing the analysis, the following key operational findings emerged: 1) no clear differences exist between the Z_{DR} column depth of tornadic and nontornadic mesocyclones, but statistically significant differences do exist between severe and nonsevere storms, 2) the lead time in advance of severe hail and wind reports provided by peaks in Z_{DR} column depth is greater than that provided by peaks in −20°C reflectivity cores, 3) increases in Z_{DR} column size precede increases in −20°C reflectivity core size by about 3.5–9.0 min, and 4) rapid-update volumetric data captures signature evolution several minutes earlier than conventional-update data therefore providing forecasters more time to anticipate hazards and issue warnings.

1. Introduction

National Weather Service (NWS) forecasters consider a vast amount of information during the warning decision process, including scientific conceptual models that help them anticipate impending hazardous weather (e.g., Andra et al. 2002; Lindley and Morgan 2004). The recent dual-polarization (dual-pol) upgrade to the Weather Surveillance Radar-1988 Doppler (WSR-88D) radar network provides an additional suite of variables and derived products that could be integrated into severe-weather conceptual models (NOAA 2013). One potentially beneficial dual-pol signature is the differential reflectivity (Z_{DR}) column. This signature may develop within a convective storm's updraft as the updraft perturbs the environmental 0°C level upward while also lofting raindrops above the 0°C level. The result is a quasi-vertical continuous column of enhanced Z_{DR} (i.e., often greater than 1 dB) that can extend well above the environmental 0°C level (e.g., Tuttle et al. 1989; Ryzhkov et al. 1994; Snyder et al. 2015).

Modeling and observational studies (e.g., Ryzhkov et al. 1994; Kumjian and Ryzhkov 2008; Kumjian et al. 2014; Snyder et al. 2015; Carlin et al. 2017) have shown that Z_{DR} columns can provide information about the location and intensity of a storm's updraft. Specifically, Kumjian et al. (2014) found a strong relationship between height of the 2-dB Z_{DR} contour and updraft magnitude at that height, and Snyder et al. (2015) found that the deepest Z_{DR} columns were associated with the strongest updrafts. This connection is relevant to NWS

Corresponding author: Charles M. Kuster, Charles.Kuster@noaa.gov

DOI: 10.1175/WAF-D-19-0024.1

forecasters because updraft and/or Z_{DR} column characteristics, such as intensity and size, have been linked to hail growth potential (e.g., Nelson 1983; Kumjian 2013), surface precipitation intensity (e.g., Picca and Ryzhkov 2010), tornado intensity (e.g., Van Den Broeke 2017), lightning activity (e.g., Deierling and Peterson 2008), and changes in low-level vorticity (e.g., Wicker and Wilhelmson 1995). Furthermore, changes in Z_{DR} column height occur prior to the time of maximum updraft intensity (Snyder et al. 2015) and observed near-surface hail cores (Picca and Ryzhkov 2010), and can therefore provide forecasters with additional time to anticipate storm intensity changes and subsequent impacts to life and property.

As knowledge about Z_{DR} columns and other dual-pol signatures increases, it is important to connect that knowledge with operational practices and conceptual models to ensure that useful signatures are efficiently used by decision makers. Conceptual models are an important piece in the warning decision process and radar data are the primary tool for detecting storm-scale features of a conceptual model (e.g., Andra et al. 2002; Brotzge and Donner 2013). In the past, new radar data has improved existing conceptual models and warning performance, so a new opportunity potentially exists with dual-pol radar data (e.g., Burgess et al. 1993; Brotzge and Donner 2013; Kumjian 2013). However, incorporating and using new data and tools can be challenging especially if sufficient background information and training does not exist and as the potential for data overload increases (e.g., Brotzge and Donner 2013). To date, research has demonstrated that Z_{DR} columns likely provide useful information about storm intensity and potential threats, but little clear information exists to connect them directly to existing conceptual models and warning decisions, thereby limiting a forecaster's ability to leverage the full benefits of dual-pol technology during severe-weather operations (e.g., Kumjian and Ryzhkov 2008; Kumjian 2013). Knowledge gaps also exist regarding Z_{DR} column evolution in nontornadic supercells, column evolution across multiple elevation angles (i.e., volumetric analysis), impact of radar update time on accurate sampling of column evolution, and typical values of Z_{DR} column depth (e.g., Van Den Broeke et al. 2008; Picca et al. 2015; Van Den Broeke 2017).

Therefore, the purpose of this study is to use rapid-update volumetric radar data to provide NWS forecasters and researchers with operationally relevant information about Z_{DR} column depth by quantifying its evolution across a wide variety of storm modes and intensities. We also relate that evolution to signatures forecasters typically use to issue severe weather warnings (e.g., upper-level reflectivity cores, mesocyclones, etc.). In addition, we seek to extend previous work (e.g., Kumjian and Ryzhkov 2008; Van Den Broeke 2017) by providing a framework that allows Z_{DR} column signatures to be integrated into existing forecaster conceptual models and the warning decision process.

TABLE 1. Number of individual storms and volume scans analyzed for each storm type.

Storm mode/characteristic	Count	Volume scans
Supercell	22	832
Single cell/multicell	20	587
Severe thunderstorm	25	934
Nonsevere thunderstorm	17	485
Tornadic mesocyclone	17	188
Nontornadic mesocyclone	23	249

This paper describes the radar data and weather events used to quantify Z_{DR} column depth evolution (section 2) and highlights operationally relevant findings (section 3). A series of subsections within section 3 address findings regarding Z_{DR} column depth of tornadic and nontornadic mesocyclones as well as severe and nonsevere storms (section 3a), the evolution of Z_{DR} column depth relative to severe hail and wind reports (section 3b), significant trends in Z_{DR} column depth that could alert forecasters to changes in storm intensity (section 3c), relationships between Z_{DR} column depth and −20°C reflectivity cores and low-level mesocyclones (section 3d), impact of radar update time on sampling Z_{DR} column depth (section 3e), and situations where effective use of Z_{DR} column depth may be limited in operations (section 3f).

2. Radar data and weather event information

To obtain radar data that can be used as a proxy for that collected by a future dual-pol phased array radar (e.g., Zrnić et al. 2007), researchers at the National Severe Storms Laboratory have been collecting rapid-update radar data for a wide variety of events with KOUN, a dual-pol WSR-88D radar located in Norman, Oklahoma. Researchers developed specialized volume coverage patterns (VCPs) and performed 90° sector scans to achieve 1.6–2.1-min volumetric updates with relatively high vertical resolution (i.e., vertical spacing generally less than 1.3 km). Our analysis of Z_{DR} column depth uses 49 storms selected from 15 different events. Of these storms, seven contained unusable Z_{DR} column depth data (section 3f), so most analysis presented in this paper focuses on 13 events that include 42 storms ranging from severe supercells to nonsevere single cells (Table 1). Of these storms, a majority were relatively isolated supercells, multicells, or single cells, but one severe and four nonsevere storms were linear in nature and one severe storm was a supercell embedded within a line. All storms were within 150 km of KOUN for

their entire life cycle and many (64%) were within 100 km. A Z_{DR} calibration was performed for every KOUN case using the presence of dry snow above the environmental melting layer similar to Picca and Ryzhkov (2012).

Two primary algorithms produced data for analysis. For Z_{DR} columns, the Z_{DR} column depth algorithm (Snyder et al. 2015) uses radar data and the environmental 0°C height from the Rapid Refresh (RAP) model (e.g., Benjamin et al. 2016) to produce a quality-controlled three-dimensional gridded field of Z_{DR} with a grid spacing of 0.0025° in latitude and longitude and 250 m in the vertical. The algorithm then uses the number of vertically consecutive grids with Z_{DR} of 1 dB or higher to calculate the depth of Z_{DR} above the environmental 0°C height and outputs those values as a two-dimensional gridded product of column depth (Fig. 1a). For upper-level reflectivity cores, we choose to analyze reflectivity at −20°C because reflectivity values at this height can be an important signal of storm intensity to forecasters (e.g., Nelson 1983; Witt et al. 1998). To create this field, the "w2merger" algorithm in the Warning Decision Support System-Integrated Information software (Lakshmanan et al. 2007) uses the environmental −20°C height from the RAP model to produce a gridded field of reflectivity at −20°C with a grid spacing of 0.0025° in latitude and longitude (Fig. 1b).

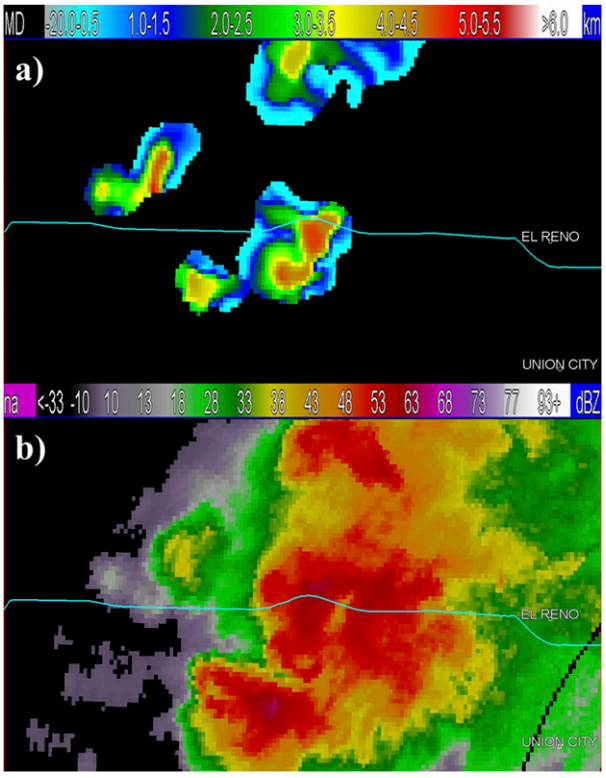

FIG. 1. Example of (a) Z_{DR} column depth and (b) −20°C reflectivity for a storm on 31 May 2013 in central Oklahoma. Range from radar at center of the images is about 75 km.

3. Radar data analysis

To quantify signature evolution, we manually extracted data from the Z_{DR} column depth and −20°C reflectivity field for each storm over its entire life cycle (i.e., Z_{DR} column development to dissipation). To assist in differentiating individual storms—especially in instances of multicell convection, merging storms, or closely spaced storms—and produce operationally relevant results, we subjectively identified thresholds and ultimately performed calculations only for Z_{DR} column depth of 1000 m or higher and −20°C reflectivity of 50 dBZ or higher. We calculated the median, maximum, and size (i.e., cross-sectional area) of each signature for all available volume scans encompassing a storm's life cycle. Since the Z_{DR} column depth algorithm requires vertical continuity, the calculated size of algorithm output represents Z_{DR} column cross-sectional area at the environmental 0°C level and is hereafter referred to as Z_{DR} column size. For low-level mesocyclone evolution, the velocity difference across the mesocyclone was calculated at the elevation angle closest to 3 km above ground level. This analysis height was chosen—despite it being on the boundary of what is typically considered as low- and midlevel—because forecasters frequently look at elevation angles around this height when diagnosing mesocyclone intensity to achieve higher warning lead times since mesocyclones and tornado vortex signatures are typically observable aloft prior to near the surface (e.g., Lemon et al. 1978; WDTD 2019).

Individual storms were classified as severe or nonsevere based on whether or not they were associated with a hail, wind, or tornado report in the National Center for Environmental Information's Storm Events Database at any time during their life cycle. Similarly, individual mesocyclones were classified as tornadic or nontornadic based upon the same verification database and the occurrence of a tornado report at any time during their life cycle. Each storm and mesocyclone was paired with a storm report based on a manual examination of the radar data. In a few instances, the storm report time was changed based on when radar data indicated a given storm actually moved over the report location. Despite our best efforts to quality control the storm reports, limitations still exist with this dataset (e.g., Trapp and Wheatley 2006) but it does provide the most robust method of storm intensity verification available.

a. *Typical values of Z_{DR} column depth*

The first step in incorporating Z_{DR} column depth into radar-based conceptual models and therefore the

warning decision process is establishing what range of values can be expected and what values might be important for anticipating severe weather. The analysis incorporated over 1400 volume scans of radar data that span a variety of environmental conditions, storm modes, storm intensities, and months (April–October), so the results presented here could be relevant to a wide variety of operational situations. However, all data came from storms in Oklahoma, so these results may be less applicable to forecast areas outside of the Southern Great Plains if regional differences exist in Z_{DR} column depth. Consequently, forecasters should be especially aware of potential differences during events with storm environments not typically seen in the Southern Great Plains (e.g., tropical environments) and during winter-season events since no such events are included in these results. Extending this work to other geographic regions and environments is an important aspect of any future research.

For all storms analyzed, 10th–90th percentile median Z_{DR} column depth ranged from 1268 to 2190 m, maximum from 1830 to 4003 m, and size from 7 to 124 km^2 (Fig. 2). Additionally, 10th–90th percentile median −20°C reflectivity ranged from 51.5 to 55.8 dBZ, maximum from 54.6 to 67.3 dBZ, and size from 0 (i.e., no 50+ dBZ core present) to 233 km^2 (not shown).

After typical values of a signature are known, an important question is whether or not the signature can be used by forecasters to distinguish between tornadic and nontornadic mesocyclones or severe and nonsevere storms in real time. We expected severe storms and tornadic mesocyclones to be associated with stronger and larger Z_{DR} columns since stronger storms typically have larger and stronger updrafts (e.g., Nelson 1983; Wicker and Wilhelmson 1995). To test this hypothesis, we used a bootstrapping method with replacement (n = 10 000) and two-sample Kolmogorov–Smirnov (KS) tests to compare statistical differences in the medians and distributions of the Z_{DR} column depth and −20°C reflectivity core metrics (e.g., median, maximum, and size) associated with all mesocyclones and storms in this dataset. Very few statistically significant differences ($p < 0.05$) existed between the Z_{DR} column depth or the −20°C reflectivity core metrics of tornadic and nontornadic mesocyclones, which we did not expect. Indeed, the two distributions for most signature metrics featured much overlap with only the two distributions of median −20°C reflectivity of tornadic and nontornadic mesocyclones being statistically distinct ($p < 0.05$, Fig. 3, Table 2). Despite the statistical significance, substantial overlap in the distributions would make it very challenging to use this radar-signature metric to distinguish between tornadic and nontornadic mesocyclones in real-time warning decisions (Fig. 3). Therefore, forecaster use of other radar metrics, such as low- to mid-level mesocyclone intensity, is likely the best practice when issuing tornado warnings.

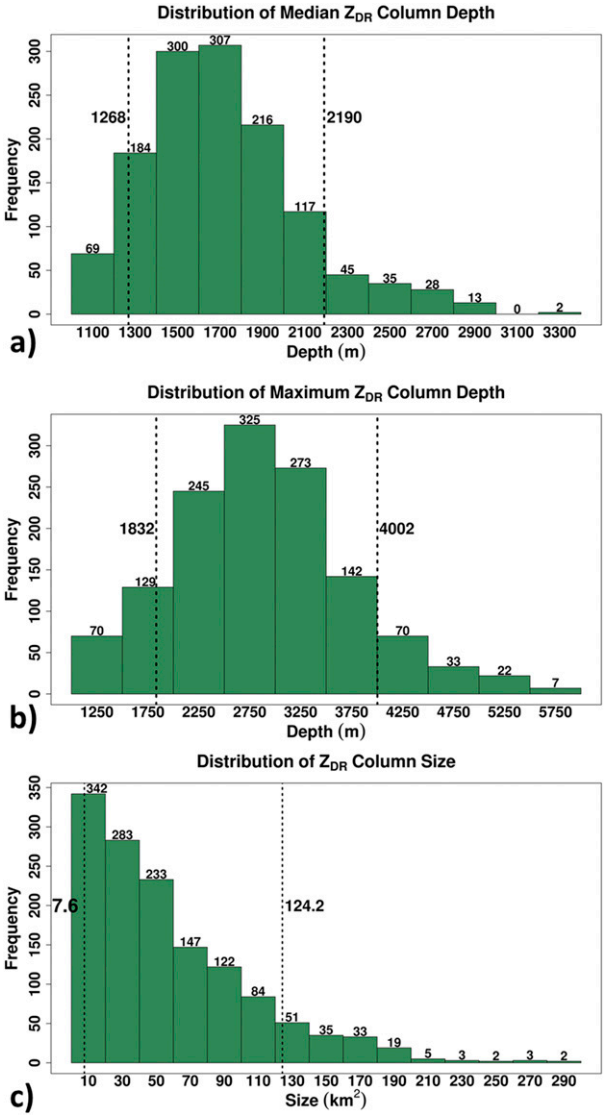

FIG. 2. Histogram of Z_{DR} column depth (a) median value, (b) maximum value, and (c) size for all volume scans (n = 1419) considered in the analysis. Histogram columns are annotated with the frequency (above), and x-axis labels are the bin midpoints. Dashed vertical lines represent the 10th and 90th percentile and are annotated with the corresponding value.

In contrast, we observed statistically significant differences between severe and nonsevere storms for all radar metrics considered as expected. The most statistically significant differences were observed when comparing the −20°C reflectivity core size of severe and nonsevere storms (Figs. 4 and 5; Table 2). For Z_{DR} column depth metrics, the most statistically significant differences

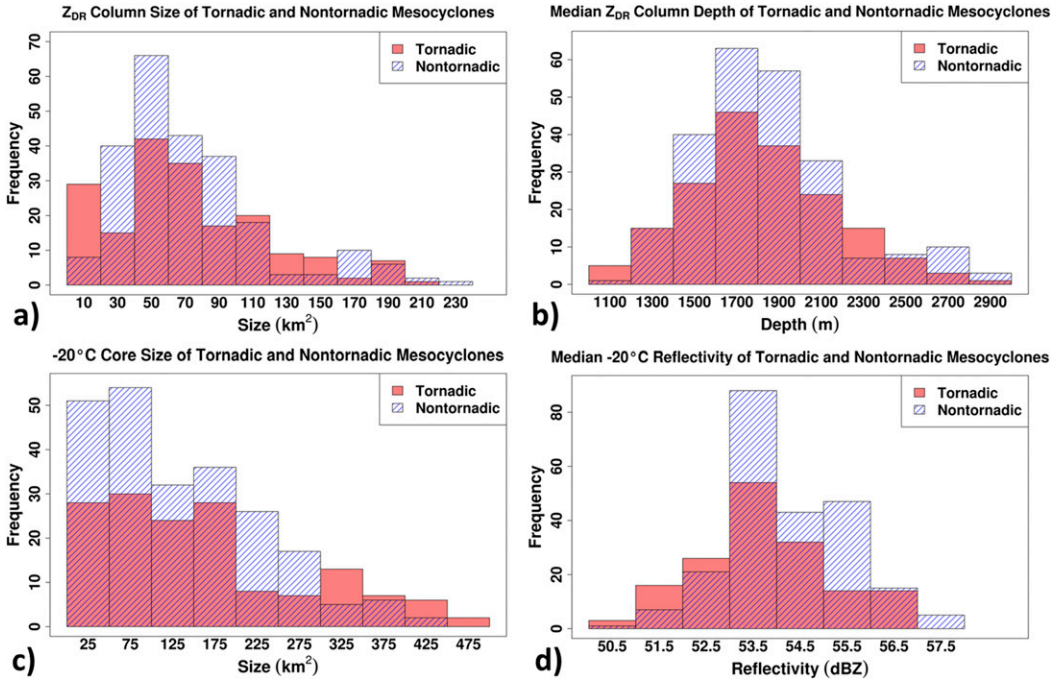

FIG. 3. Distribution of (a) Z_{DR} column size, (b) median Z_{DR} column depth, (c) −20°C reflectivity core size, and (d) median −20°C reflectivity for all volume scans (n = 437) of tornadic (red columns) and nontornadic (blue hatched columns) mesocyclones considered in the analysis. Bin midpoints are included as the x-axis labels.

were observed when comparing the column size of severe and nonsevere storms, but these differences were less statistically significant than all −20°C reflectivity core metrics (Figs. 4 and 5; Table 2).

Since statistically significant differences between the Z_{DR} column depth and −20°C reflectivity cores of severe and nonsevere storms were common in this sample, considering the distributions of these radar metrics might help forecasters distinguish between severe and nonsevere storms, especially when certain thresholds are exceeded. For example, in this dataset, once Z_{DR} column size reached 60 km^2 or maximum Z_{DR} column depth reached 3100 m, at least 71.1% and 66.7% of the volume scans were associated with severe storms, respectively (Figs. 6a,b). Similarly, once −20°C reflectivity core size reached 75 km^2 or maximum −20°C reflectivity

TABLE 2. Measures of statistical significance for differences between tornadic and nontornadic mesocyclones (tornadic − nontornadic) and severe and nonsevere thunderstorms (severe − nonsevere). Observed differences larger (in magnitude) than the 95th percentile bootstrapping method differences or with KS test p values < 0.05 were considered statistically significant and are indicated by **.

Radar signature metric	95th percentile bootstrapping method differences	Observed difference in radar signature medians	KS test p value
		Tornadic vs nontornadic mesocyclones	
Z_{DR} column size	8.8 km^2	0.9 km^2	0.06
Median Z_{DR} column depth	−59.2 m	−5.2 m	0.58
Max Z_{DR} column depth	−124.0 m	−52.7 m	0.33
Reflectivity core size	33.3 km^2	25.5 km^2	0.04
Median reflectivity**	−0.2 dBZ	−0.3 dBZ	<0.01
Max reflectivity**	−0.9 dBZ	−0.5 dBZ	<0.01
		Severe vs nonsevere thunderstorms	
Z_{DR} column size**	5.6 km^2	31.2 km^2	<0.01
Median Z_{DR} column depth**	52.8 m	193.6 m	<0.01
Max Z_{DR} column depth**	130.8 m	549.1 m	<0.01
Reflectivity core size	8.4 km^2	71.4 km^2	<0.01
Median reflectivity**	0.2 dBZ	1.4 dBZ	<0.01
Max reflectivity**	0.8 dBZ	5.2 dBZ	<0.01

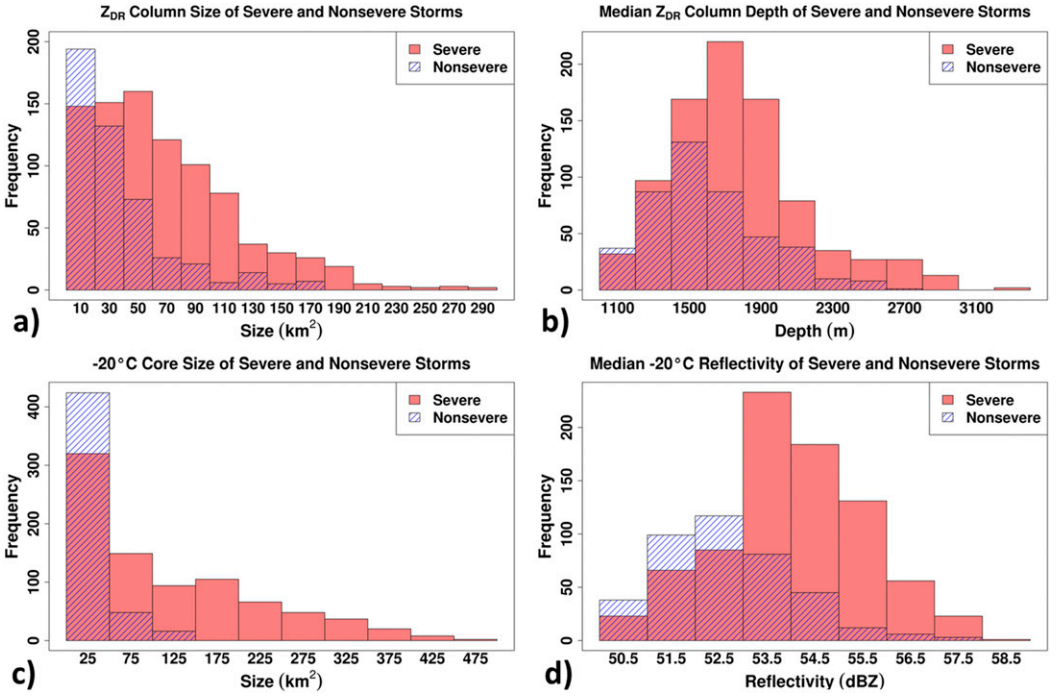

FIG. 4. As in Fig. 3, but comparing all volume scans of severe (n = 934) and nonsevere (n = 485) storms considered in the analysis.

reached 62 dBZ, at least 71.7% and 69.4% of volume scans were associated with severe storms, respectively (Figs. 6c,d). In addition, once −20°C reflectivity core size exceeded 125 km^2 (~73rd percentile) and Z_{DR} column size exceeded 180 km^2 (~97th percentile), all storms in this dataset were severe. Such an observation, potentially provided by algorithms, combined with trend information (section 3c) could signal to a forecaster that a severe thunderstorm warning may be needed.

Use of any radar-based threshold (e.g., Z_{DR} column size higher than 60 km^2) can increase confidence that a given storm is severe, but radar characteristics of storms typically occur along a continuous spectrum and rarely fall neatly into two distinct categories (e.g., Smith et al. 2015). In this dataset, volume scans of severe storms occurred at nearly every threshold and overlap occurred between severe and nonsevere storms for all radar metrics (Figs. 4–6). For example, if a forecaster used a Z_{DR} column size threshold of 60 km^2 to issue warnings, 71% of the volume scans in this dataset were associated with severe storms, but 52% of severe storm volume scans also fell below this threshold and would therefore be missed by warnings. In this case, most volume scans exceeding this threshold were severe, but many severe storm volume scans did not meet this threshold. This realization combined with the percentage of severe storm volume scans at each threshold (Figs. 4 and 6) could give forecasters a starting point for determining what thresholds might be most suitable for issuing severe thunderstorm warnings based on Z_{DR} column depth. Other warning-decision thresholds (e.g., 50 dBZ to 30 kft), storm reports, postevent verification, machine learning methods, and environmental characteristics may also be used to refine this threshold in an operational setting.

b. *Signature evolution relative to severe hail and wind reports*

After determining that Z_{DR} column depth was not necessarily a better distinguisher of storm severity than −20°C reflectivity cores, we next examined the timing of signature evolution relative to severe weather reports for potential operational implications. From an operational and research perspective, it is important to consider whether or not additional radar signatures provide enough beneficial information to warrant use during warning operations especially when many other factors require forecaster attention (e.g., Andra et al. 2002; Heinselman et al. 2012; Wilson et al. 2017). Since results from previous research (e.g., Picca and Ryzhkov 2010; Kumjian et al. 2014; Snyder et al. 2015) suggest that Z_{DR} columns are an early indicator of updraft and surface-precipitation intensity, we analyzed Z_{DR} column depth and −20°C reflectivity core evolution prior to all severe hail (n = 21) and wind (n = 11) reports where signature metric data were complete. Any report

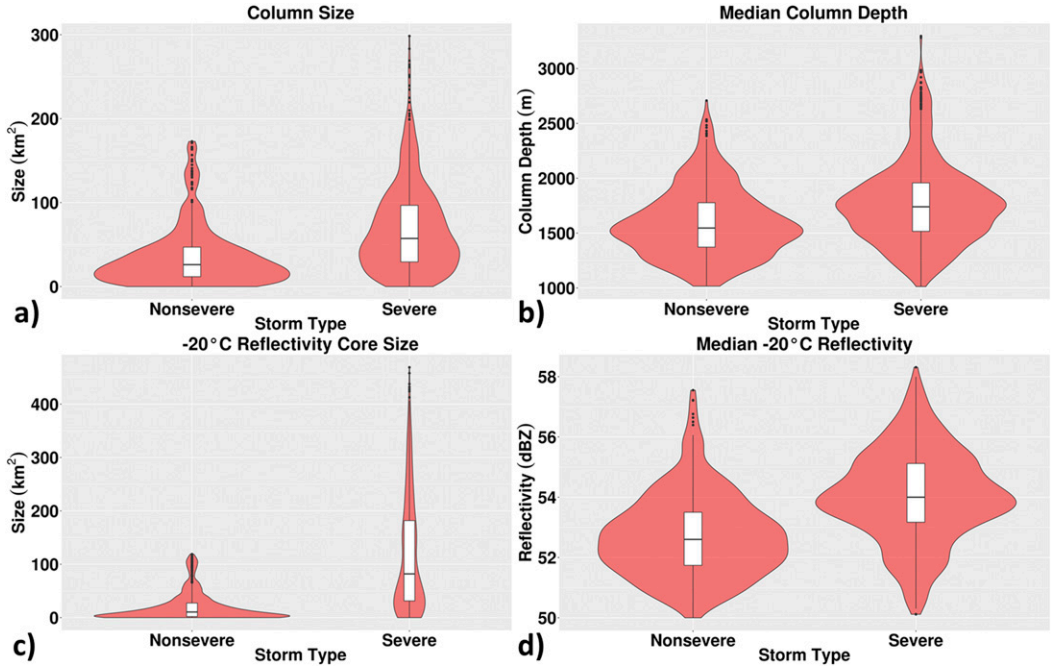

FIG. 5. Violin plots of (a) Z_{DR} column size, (b) median Z_{DR} column depth, (c) −20°C reflectivity core size, and (d) median −20°C reflectivity. The red area of the plot shows the probability density with a greater width indicating a higher frequency of occurrence. Associated box plots are included within each violin plot for reference. Box edges are the lower (Q1) and upper (Q3) quartiles, the horizontal black line is the median, and outliers are indicated by black dots.

not preceded by at least 15 min of KOUN data was not considered in the analysis.

Peaks (i.e., local maxima) in Z_{DR} column size typically occurred earlier and more frequently prior to severe hail and wind reports than peaks in −20°C reflectivity core size (Fig. 7). This result is not surprising since Z_{DR} columns are associated with developing updrafts whereas reflectivity cores are associated with greater hydrometeor sizes and concentrations that develop as a result of the updraft (e.g., Kumjian et al. 2014; Snyder et al. 2015). The largest lead time in this study occurred with peaks in Z_{DR} column size, where peaks occurred about 7 min (median value) prior to severe hail reports (Fig. 7a) and about 9 min (median value) prior to severe wind reports (Fig. 7b). These lead times are somewhat shorter than previous studies (e.g., Picca and Ryzhkov 2010; Snyder et al. 2015) but we expect they would be longer if based on increasing trends in signature metrics rather than peak timing. Peaks in Z_{DR} column size also occurred about 6.5 and 9 min earlier than peaks in −20°C reflectivity core size for severe hail and wind reports, respectively. About 76% (16/21) of severe hail reports and 82% (9/11) of wind reports were preceded by a peak in Z_{DR} column size, whereas only 50% (10/20) of severe hail reports and 22% (2/9) of severe wind reports were preceded by a peak in −20°C reflectivity core size. Similar patterns were generally observed when comparing median and maximum Z_{DR} column depth and −20°C reflectivity, but these were not as pronounced as those observed with signature size (Fig. 7).

The higher frequency of occurrence and additional lead time provided by Z_{DR} column depth evolution could be useful to forecasters because it provides them with more time to interrogate potentially threatening storms and issue warnings prior to severe weather impacts at the ground. Using Z_{DR} column depth could also be beneficial because, although −20°C reflectivity core size was the best discriminator between severe and nonsevere storms (section 3a), it provided the least amount of lead time and preceded less than 50% of severe reports, while Z_{DR} column size provided the longest lead time and preceded more than 75% of severe reports (Fig. 7). This difference in lead time is especially noteworthy for severe wind reports because −20°C reflectivity core sizes provided zero median lead time for the events in this study. Therefore, using Z_{DR} column depth in tandem with −20°C reflectivity cores could help forecasters more effectively anticipate impending hazardous weather.

c. *Significant signature peaks*

Numerous Z_{DR} column depth and −20°C reflectivity core peaks occurred with the storms analyzed in this

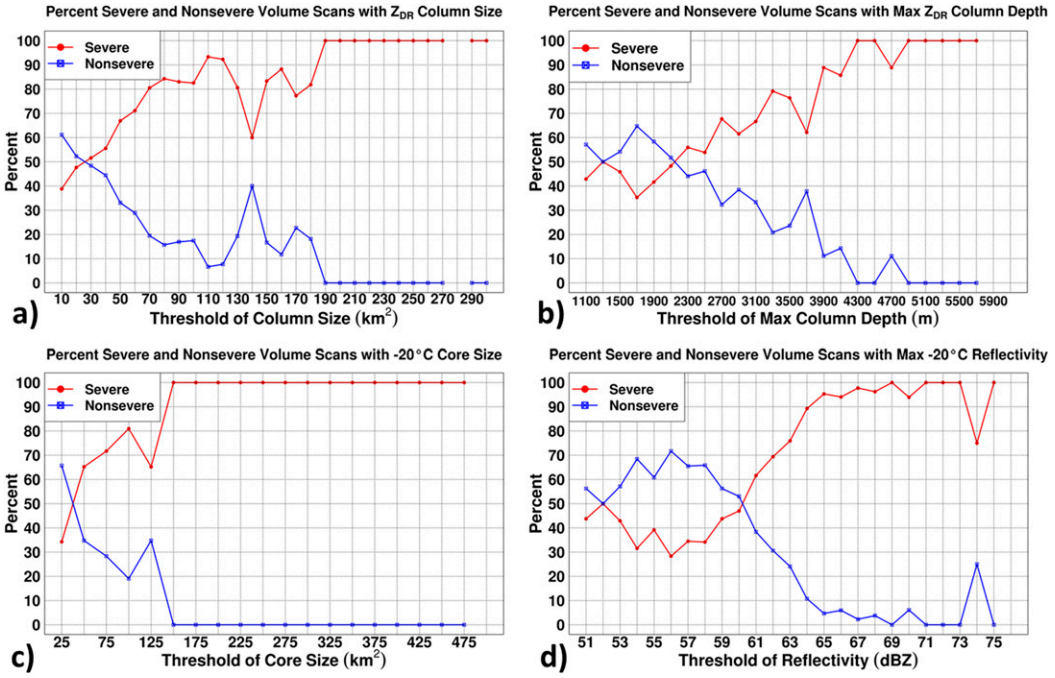

FIG. 6. Percent of all volume scans that were associated with severe (red line) and nonsevere (blue line) storms at various thresholds for (a) Z_{DR} column size, (b) maximum Z_{DR} column depth, (c) −20°C reflectivity core size, and (d) maximum −20°C reflectivity.

study, but most peaks were short-lived, had low amplitudes (i.e., only small increase in size or median values), and were not associated with severe weather reports (i.e., could produce false alarms). Therefore, it could be challenging for forecasters to determine which increasing trends and peaks are worth paying attention to during real-time warning operations. As a first look into addressing this challenge and quantifying Z_{DR} column depth over operationally relevant time scales, we calculated the distribution of changes in Z_{DR} column depth metrics over three and five volume scans (about 5.5–9 min). This time scale was chosen because many of the observed peaks occurred in 10 min or less and forecasters typically make warning decisions about a given storm in this amount of time.

To highlight trends that might be most relevant to operations, we calculated thresholds and percentiles that included at least 75% of the 21 severe hail reports in this dataset (Table 3). For example, 75% of hail reports were associated with an increase in Z_{DR} column size of at least 23.7 km^2 over three volume scans. This delta value of Z_{DR} column size was therefore considered significant and corresponded to the 80th percentile of all changes in column size over three volume scans (Fig. 8a). Radar metric delta values with higher percentiles are likely more relevant to forecasters since the small, low-amplitude, transient peaks are less likely to be associated with hazardous weather and could be ignored, which would allow forecasters to retain special attention for storms that might pose a greater risk for severe hail at the surface. In this dataset, the highest percentiles occurred with Z_{DR} column size and −20°C reflectivity core size over three volume scans (Fig. 8; Table 3). Many instances of Z_{DR} column size increasing by at least 23.7 km^2 also occurred without a hail report, however, so this analysis is meant to draw attention toward the upper end of the observed delta distributions rather than provide an explicit threshold for warning decisions. A larger sample of storms and hail reports is needed to better determine operationally relevant trend thresholds, but this study provides a potential starting point.

d. Connecting Z_{DR} columns with existing conceptual models: Evolution relative to −20°C reflectivity cores and low-level mesocyclones

Scientific conceptual models help forecasters anticipate hazards and issue warnings (e.g., Andra et al. 2002), so we expect that integrating new dual-pol radar signatures and products into existing conceptual models will result in more effective and more frequent use during the warning decision process. Therefore, in addition to examining typical values of Z_{DR} column depth and its evolution compared to storm reports, we also looked for relationships between Z_{DR} column depth and radar

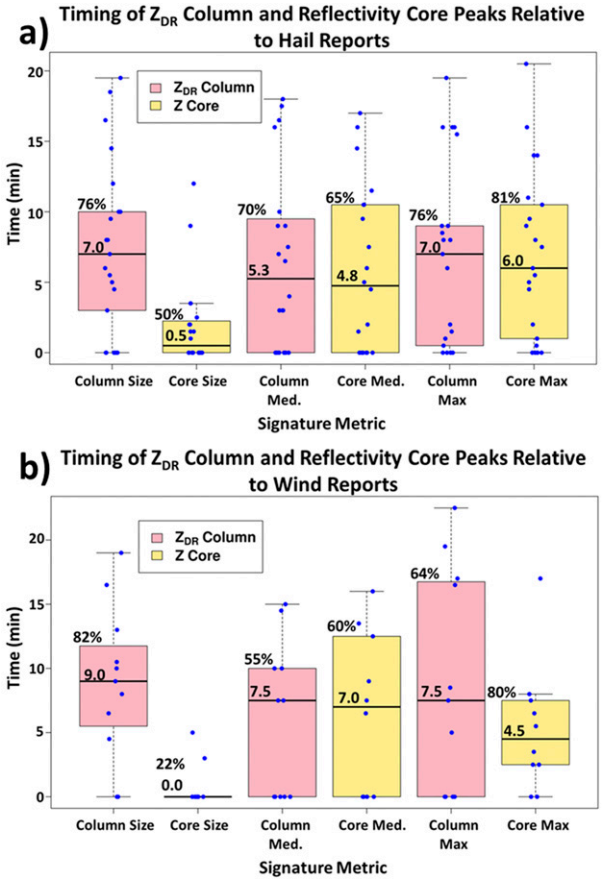

FIG. 7. Boxplot showing amount of time signature peaks occurred prior to (a) severe hail reports and (b) severe wind reports. Percent of reports preceded by a signature peak and median lead times are annotated above and within each box, respectively. Box edges are the lower (Q1) and upper (Q3) quartiles, the horizontal black line is the median, and the lower and upper whiskers represent Q1 − 1.5 × IQR and Q3 + 1.5 × IQR, respectively, where IQR is the interquartile range. Blue dots indicate data used in boxplot creation.

signatures that already exist within forecaster radar-based conceptual models, such as −20°C reflectivity cores and low-level mesocyclones. To do this, we employed lag correlations to quantify potential relationships between radar signatures because changes in Z_{DR} column depth likely occur before changes in −20°C reflectivity cores (e.g., Knight 2006; Picca and Ryzhkov 2010) and also perhaps before changes in updraft intensity and therefore low-level mesocyclones (e.g., Wicker and Wilhelmson 1995). Similarly to section 3a, significance of the lag correlations was done using a bootstrapping method with replacement ($n = 5000$).

The analysis revealed that strong relationships did not exist between median or maximum Z_{DR} column depth and −20°C reflectivity in this dataset. However, a means for operationally linking these signatures does appear to exist when considering signature size. We observed statistically significant lag correlations for all lags between 0 and −8 volume scans (a negative lag means that Z_{DR} column size precedes −20°C reflectivity core size), with the maximum occurring at lag −4 ($r = 0.21$; $p < 0.05$) and the highest 4 correlations occurring between lag −2 and lag −5 (Fig. 9a). Assuming an average volume update time of 1.8 min across all KOUN cases, these lags correspond to lag times of about 7 min for the maximum correlation and about 3.5–9 min for the highest four correlations. Operationally speaking, based on these data, if a forecaster sees an increase in Z_{DR} column size, they can expect an increase in −20°C reflectivity core size about 3.5–9 min later. This additional time is important in two ways. First, it could give a forecaster additional time to interrogate a given storm and be prepared to issue a warning once critical reflectivity thresholds are met. Second, if certain thresholds of Z_{DR} column depth are exceeded (section 3a) and if warranted by the environmental conditions, a forecaster could have increased confidence in issuing a warning prior to intensification of the −20°C reflectivity core. In this scenario, a forecaster would be able to leverage the finding that peaks in Z_{DR} column size typically occur earlier prior to severe hail and wind reports than peaks in −20°C reflectivity core size to potentially increase severe thunderstorm warning lead time (section 3b).

Greater volume scan to volume scan consistency (i.e., less variability) offers one potential explanation for why signature size was the only metric to provide an operationally relevant relationship between Z_{DR} column depth and −20°C reflectivity cores. The autocorrelation functions for maximum and especially median Z_{DR} column depth decreased quickly (not shown), whereas the autocorrelation function for Z_{DR} column size decreased more gradually (Fig. 9b). This observation suggests that there is more variability and fewer

TABLE 3. Trend threshold (delta) and percentile encompassing 75% of severe hail reports for each radar metric considered over three and five volume scans (about 5.5 and 9 min, respectively).

Radar metric (No. of volume scans)	Trend threshold	Percentile
Z_{DR} column depth size (3)	23.7 km^2	80.2
Z_{DR} column depth size (5)	27.3 km^2	77.5
Median Z_{DR} column depth (3)	236 m	63.5
Median Z_{DR} column depth (5)	282 m	64.5
Max Z_{DR} column depth (3)	710 m	77.3
Max Z_{DR} column depth (5)	710 m	72.8
−20°C core size (3)	21.8 km^2	78.5
−20°C core size (5)	29.1 km^2	77.5
Median −20°C reflectivity (3)	1.3 dBZ	76.2
Median −20°C reflectivity (5)	1.5 dBZ	76.0
Max −20°C reflectivity (3)	3.2 dBZ	74.3
Max −20°C reflectivity (5)	3.6 dBZ	73.1

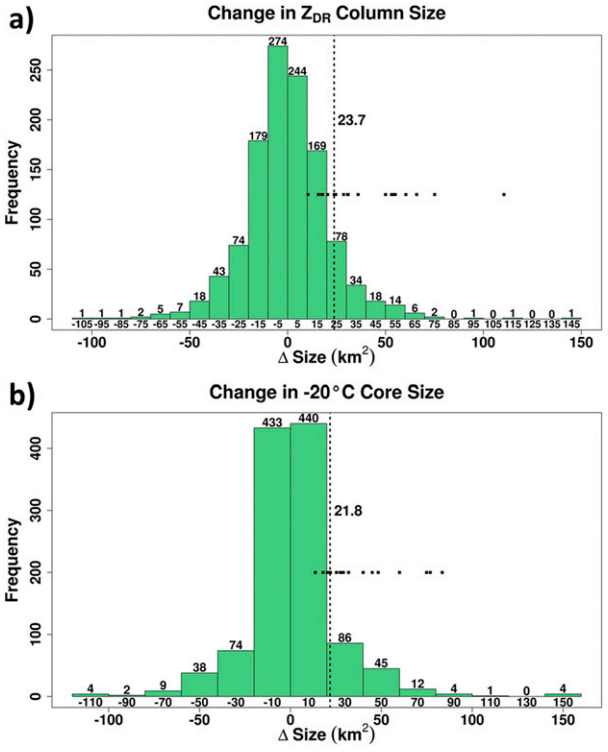

FIG. 8. Histogram of changes in (a) Z_{DR} column size and (b) −20°C reflectivity core size over three volume scans (about six min). Vertical dashed line indicates the threshold at which at least 75% of the hail reports (indicated by black dots) occur and is annotated with its value. Histogram columns are annotated with the bin midpoint (below) and frequency (above).

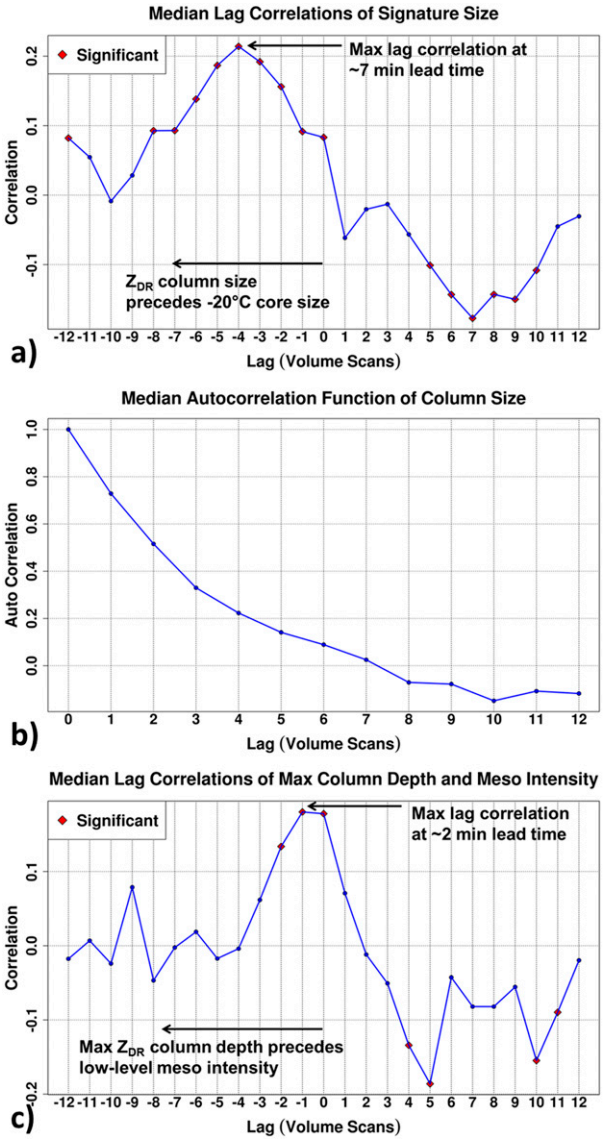

FIG. 9. Median (a) lag correlations between Z_{DR} column and −20°C reflectivity core size, (b) autocorrelation function for Z_{DR} column size, and (c) lag correlations between maximum Z_{DR} column depth and low-level mesocyclone intensity (i.e., velocity difference). In (a) and (c), red markers indicate statistical significance (95% confidence) and negative lag times indicate that Z_{DR} column depth evolution precedes −20°C reflectivity core size and low-level mesocyclone intensity, respectively.

patterns when looking at median and maximum Z_{DR} column depth, which helps explain the lack of clear relationships between those metrics and −20°C reflectivity cores. This result was also supported when looking at data for individual storms separately, where patterns were more readily observed when looking at Z_{DR} column size rather than median or maximum values. In agreement with Van Den Broeke (2017) and studies linking updraft width and hail growth (e.g., Foote 1984), we believe that it may be important for forecasters to pay special attention to Z_{DR} column and −20°C reflectivity core size when interrogating radar data. Since size is a difficult metric to quantify in real time when looking at radar displays in the Advanced Weather Interactive Processing System (AWIPS; e.g., Andra et al. 2002), developing algorithms that can track storms (e.g., Lakshmanan et al. 2009), calculate signature size, and display that information to forecasters within AWIPS is an important step forward.

We only observed weak relationships (if any) between Z_{DR} column depth and mesocyclone intensity. Maximum Z_{DR} column depth provided the most robust relationship between the signatures. It is possible that maximum Z_{DR} column depth increases at about the same time or up to two volume scans (about 3.5 min) earlier than an increase in mesocyclone intensity (Fig. 9c). We also did not observe any clear relationships between Z_{DR} column depth or −20°C reflectivity core metrics and a tornado's enhanced Fujita (EF) scale rating. This result does differ from that found in Van Den Broeke (2017), but our sample size is small (17 tornadoes present during 188 volume scans), which likely impacts these results.

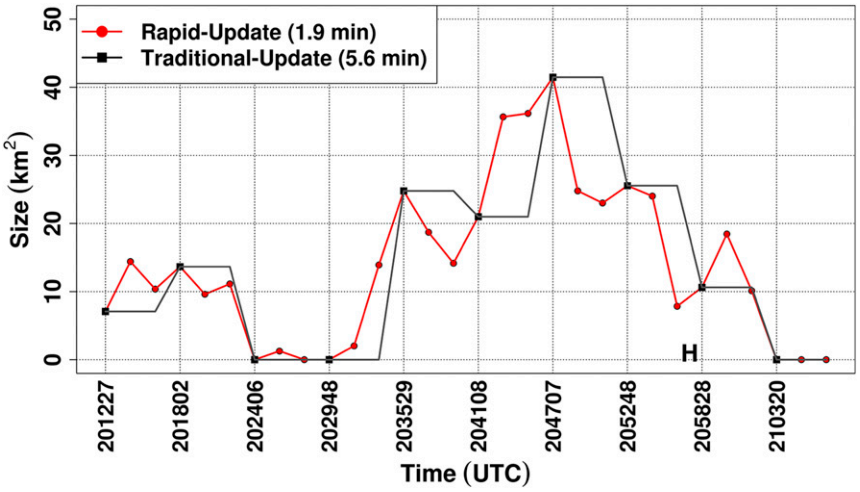

FIG. 10. Time series of Z_{DR} column size sampled by rapid-update (<1.9-min volumes) KOUN data (red line) and degraded (5.6-min volumes) KOUN data (gray line) for a hail-producing supercell on 9 May 2016. The letter H indicates time of severe hail report.

Future work could increase the sample size of tornadic supercells, but it is possible that the greatest operational benefits of Z_{DR} columns relate to severe and nonsevere storms rather than tornadic and nontornadic ones.

e. *Impact of radar update time*

With the ongoing development of rapid-update phased array radar systems (e.g., Forsyth et al. 2005; Zrnić et al. 2007) and the potential benefits rapid-update data could provide to forecasters (e.g., Heinselman et al. 2008, 2012; Wilson et al. 2017), radar update time is an important factor to consider for operational applications. Since all data used in this study were "rapid update" (volumetric update time < 2.1 min) compared to conventional WSR-88D scanning strategies, this dataset also provides an opportunity to examine the impact of radar update time on sampling Z_{DR} column depth and −20°C reflectivity cores. Therefore, we explored impacts of different volumetric update times on Z_{DR} column depth and −20°C reflectivity cores by comparing unaltered (volumetric update time < 2.1 min) and degraded (volumetric update time of 5–6 min) KOUN data.

Our analysis showed that rapid-update data were beneficial in capturing a more complete picture of signature evolution as well as providing additional lead time prior to severe hail and wind reports. A severe hail-producing, nontornadic supercell on 9 May 2016 provides one example where rapid updates better sampled Z_{DR} column size evolution (Fig. 10). Beginning at 2031:41 UTC, rapid-update KOUN data showed an increasing trend in Z_{DR} column size that persisted for the next two volume scans (about 4 min). The degraded KOUN data—representative of a forecaster using data with traditional volumetric update times—did not depict this increasing trend until about 4 min later at 2035:29 UTC. Afterward, a short period of decreasing Z_{DR} column size occurred, which caused the degraded KOUN data to show a decreasing trend in Z_{DR} column size by 2041:08 UTC. However, the rapid-update KOUN data showed that the decreasing trend had ended by this time and Z_{DR} column size was actually rapidly increasing. A forecaster using degraded KOUN data would not have known about the increasing trend until 2047:07 UTC. Immediately after 2047:07 UTC, rapid-update KOUN data depicted a clear decreasing trend that was not sampled by the degraded KOUN data until about 5.5 min later at 2052:48. Based on the differing sampling of these trends, a forecaster using rapid-update KOUN data would be aware of a peak in Z_{DR} column size about four min earlier than if using degraded KOUN data. All other factors being equal, the later sampling of these Z_{DR} column size evolutions could delay a warning decision and decrease lead time for the 1.75-in. (4.4 cm) hail that occurred at 2057 UTC (Fig. 10).

Rapid-update data provided a more complete picture of signature evolution, thereby enhancing the prognostic capability of Z_{DR} columns. For severe hail reports, median lead time (i.e., time between severe report and radar-signature peak) of Z_{DR} column size and median depth was 4.0 and 5.3 min longer for rapid-update data than traditional-update data, respectively (Fig. 11a). For severe wind reports, median lead time of Z_{DR} column size and median depth was 7.5 and 7.0 min longer for rapid-update data than traditional-update data, respectively (Fig. 11b). This additional time could help forecasters better analyze observed trends and anticipate upcoming hazards and changes in storm intensity.

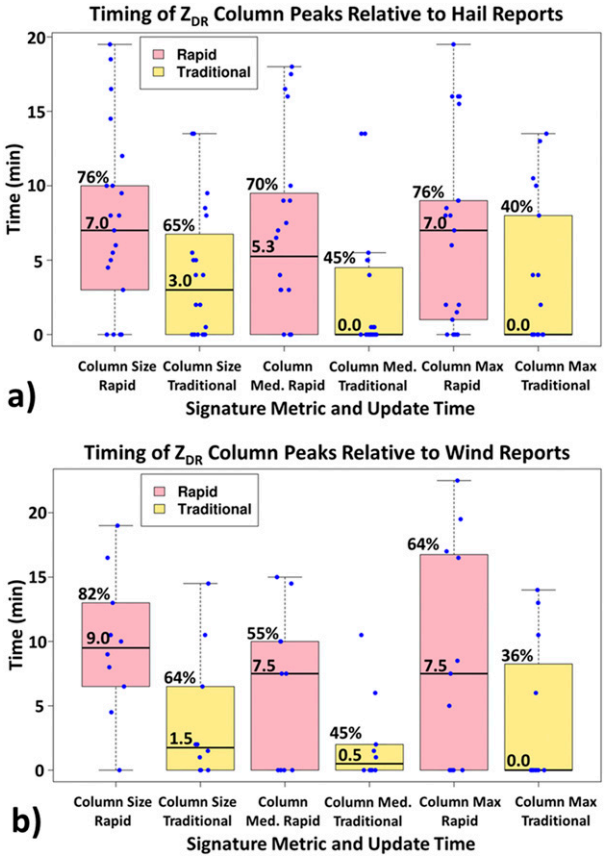

FIG. 11. As in Fig. 7, but comparing time between signature peaks and severe weather reports between rapid-update (<2-min volumes) KOUN data and traditional-update (5–6-min volumes) KOUN data.

Since radar update time impacts how forecasters are able to identify and analyze storm features, it is important to consider volumetric update time when choosing an operational radar scanning strategy. In instances where mid- to upper-level features such as Z_{DR} columns, −20°C reflectivity cores, and midlevel mesocyclones provide vital information for warning decisions, selecting a scanning strategy with the fastest volumetric update time would likely be most beneficial. Scanning strategies such as the Supplemental Adaptive Intravolume Low-Level Scans (SAILS; Crum et al. 2013) decrease update time for the lowest elevation angle, but increase total volumetric update time, so SAILS may not be beneficial in every situation (Heinselman et al. 2015). This ''trade-off'' between more frequent low-level scans and less frequent volume scans should be considered carefully, since the ability to analyze mid to upper-level radar signatures and algorithms that require data above the lowest elevation angle may be negatively impacted when more time is required to complete a full volume scan. Therefore, it is likely best for each forecast office and forecaster to generally consider what radar signatures might be most important for warning decisions during each phase of storm evolution and then select WSR-88D scanning strategies accordingly. Innovative new WSR-88D scanning strategies and new radar technology, such as phased array radars, could also decrease volumetric update time and improve sampling of important midlevel radar signatures.

f. Situations that could limit effective operational use of Z_{DR} columns

While analyzing this dataset, we noticed some situations where using Z_{DR} columns to gain more information about a storm would likely not be possible. Six supercells (four ''right movers'' and two ''left movers'') in our study were prolific hail producers and either had very small or nonexistent Z_{DR} columns. We hypothesize that hail falling back into the updraft reduced the Z_{DR} above the melting layer and prevented the radar from detecting a robust Z_{DR} column because the presence of large hail with ~0-dB Z_{DR} may have masked the presence of raindrops or wet hail with higher Z_{DR} (e.g., Kumjian et al. 2014). Forecasters should be aware that storms producing abundant hail may not exhibit clear Z_{DR} columns (Fig. 12). Three-body scatter spikes (e.g., Lemon 1998) and tornadic debris signatures can also mask Z_{DR} columns and severely reduce the utility of the Z_{DR} column depth algorithm.

When considering thresholds of Z_{DR} column depth for warning purposes, forecasters must remain aware of each storm's environment—as is good practice in any situation. One clear example in our dataset occurred on 31 May 2013 when training supercells had similar Z_{DR} column sizes but produced tornadoes of vastly different intensity. The leading supercell (''Supercell1'') produced an EF3 tornado that was 2.6 mi (4.2 km) wide (Bluestein et al. 2015). The second supercell (''Supercell2'') produced a short-lived EF0 tornado despite having a larger Z_{DR} column size over the storm's life cycle than the leading supercell (Fig. 13). We suspect that rain-cooled outflow from the leading supercell decreased low-level buoyancy of inflow air for the second supercell leading to a much weaker low-level mesocyclone and tornado. This difference and other mesoscale environmental differences must be monitored in addition to radar data for effective and accurate anticipation of hazardous weather (Andra et al. 2002).

4. Summary

The purpose of this study is to provide NWS forecasters with useful information and guidance about the potential use of Z_{DR} column depth in operations by examining its evolution over a relatively wide range of

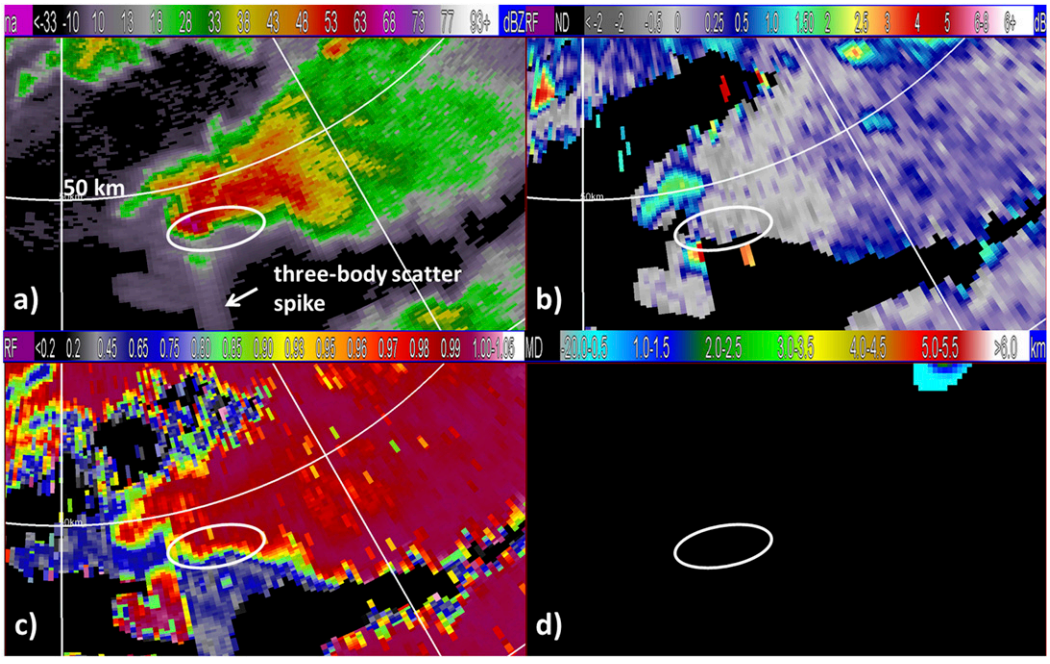

FIG. 12. Example of a prolific hail-producing storm on 26 Mar 2017 in terms of (a) reflectivity, (b) Z_{DR}, (c) correlation coefficient, and (d) Z_{DR} column depth at the 1.40° elevation angle (about 2.5 km above radar level). White ovals indicate expected location for a Z_{DR} column and output from the Z_{DR} column depth algorithm, but neither exists perhaps due to hail falling into the updraft and presence of a three-body scatter spike. White curved line in (a)–(c) is the 50-km range ring, while straight white lines indicate a 30° change in azimuth.

storm modes and intensities and comparing it with signatures typically used by forecasters during the warning decision process. Our goal is to help forecasters integrate Z_{DR} column information into existing conceptual models because such an effort is likely to result in any radar signature being used more often and more effectively in operations. To that end, after an analysis of rapid-update dual-pol radar data for 42 storms, we conclude the following for this dataset of storms in Oklahoma:

1) Distributions of Z_{DR} column depth and −20°C reflectivity core metrics are very similar between tornadic and nontornadic mesocyclones (Fig. 3), so their use is unlikely to improve tornado warning decision making.
2) Statistically significant differences exist between severe and nonsevere storms in terms of the Z_{DR} column depth and −20°C reflectivity core metrics, indicating that these products can provide forecasters with information to improve severe thunderstorm warning decisions.
3) In general, Z_{DR} column size increases prior to increases in −20°C reflectivity core size and can provide an additional 3.5–9.0 min to interrogate storm characteristics and issue warnings, thereby potentially aiding forecasters in increasing severe thunderstorm warning lead time on the order of about 5 min for all storms including less organized nonsupercell convective modes.
4) The Z_{DR} column size and −20°C reflectivity core size provide a way to relate these signatures and potentially integrate Z_{DR} columns into existing forecaster conceptual models and by extension, the warning decision process.
5) The Z_{DR} column size and −20°C reflectivity core size are the best discriminators between severe and nonsevere storms, provide the longest lead time for severe hail and wind reports, and are less variable than

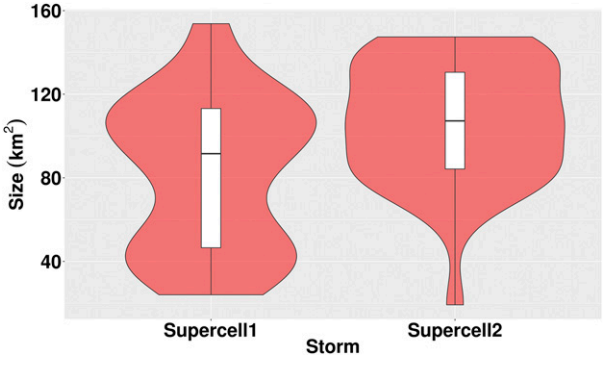

FIG. 13. Violin plots of Z_{DR} column size for two supercells occurring on 31 May 2013. Violin plot convention is the same as in Fig. 5.

signature median and maximum, so signature size could provide forecasters with the most information and clearest picture of storm evolution.

6) Rapid-update data (i.e., <2-min volumes) is advantageous for measuring Z_{DR} column depth and −20°C reflectivity cores because it samples signature evolution earlier and more completely, which provides additional time for anticipating storm hazards.

There are several important operational considerations to remember when interpreting and applying the results of this study. First, despite a relatively wide range of environments and storm modes considered, all data were from Oklahoma, so the results may not be generalizable to other geographic regions. Second, as of the publication date, a Z_{DR} column depth algorithm is not available operationally. Forecasters would therefore need to examine all tilts and roughly monitor changes in the depth of the 1.0-dB Z_{DR} isosurface within a Z_{DR} column to identify deepening columns. One can observe increases in Z_{DR} column depth prior to changes in upper-level reflectivity cores without the Z_{DR} column depth algorithm, but the algorithm provides a means to see depth information without examining multiple elevation angles and would save forecasters time especially during active severe weather events. Therefore, future endeavors should work to make the Z_{DR} column depth algorithm available to NWS forecasters in real time. Once available, it is important to remember that algorithm output is affected by the VCP's vertical resolution, and therefore a storm's range from the radar, as well as the radar's Z_{DR} calibration.

Additionally, the results of this study are based on rapid-update data (i.e., about 2-min volumes), which are currently not available to NWS forecasters. However, we examined typical values, statistical significance between severe and nonsevere storms, and percentage of severe and nonsevere storms at various radar metric thresholds (section 3a) using unaltered and degraded KOUN data, and the results were similar. This finding suggests that the conclusions of this study are still relevant to NWS operations today, but rapid-update volumetric radar data provides a more complete view of Z_{DR} column evolution, which could explain the larger observed differences between the Z_{DR} column depth of severe and nonsevere storms when using rapid-update KOUN data. This information, combined with the results provided in section 3e, suggest that considering new methods and technologies to decrease radar volumetric update time will likely benefit NWS warning operations. Additionally, rapid-update, volumetric, dual-pol radar data are also likely to benefit convective-allowing forecast models used in a future Warn-on-Forecast system (e.g., Jung et al. 2008; Supinie et al. 2017).

Acknowledgments. I thank God for giving me the opportunity and talented research team to accomplish this work. Specifically, the authors thank John Krause for help with Perl programming; Eddie Forren for KOUN data processing; Danny Wasielewski, Micheal Shattuck, Allen Zahrai, and Rafael Mendoza for KOUN data collection support; and five NWS Norman Forecast Office employees (Ryan Barnes, Randy Bowers, Vivek Mahale, Richard Smith, and Doug Speheger) for providing operational guidance on radar data analysis. We also thank Karen Cooper for help with WDSS-II; Emma Kuster for support and helpful feedback on research ideas and manuscript figures; Katie Wilson for insightful conversations and research ideas; Tanya Riley, Tracy Reinke, Jamie Foucher, and Colleen Hickman for help with administrative logistics; Chris Carter, Steve Fletcher, Jeff Horn, Brian Moore, Brett Morrow, Zachary Ross, Zach Tomek, Seth Young, and everyone at NSSL IT for help with computer hardware/software issues; and Jacob Carlin, Chris Schwarz, and Jami Boettcher for reviewing and improving the manuscript. We also thank three anonymous reviewers for helping us greatly improve the quality of this manuscript. Funding for CK, TS, JB, and RT was provided by NOAA/Office of Oceanic and Atmospheric Research under NOAA-University of Oklahoma Cooperative Agreement NA16OAR4320115, U.S. Department of Commerce.

REFERENCES

Andra, D. L., E. M. Quoetone, and W. F. Bunting, 2002: Warning decision making: The relative roles of conceptual models, technology, strategy, and forecaster expertise on 3 May 1999. *Wea. Forecasting*, **17**, 559–566, https://doi.org/10.1175/1520-0434(2002)017<0559:WDMTRR>2.0.CO;2.

Benjamin, S. G., and Coauthors, 2016: A North American hourly assimilation and model forecast cycle: The Rapid Refresh. *Mon. Wea. Rev.*, **144**, 1669–1694, https://doi.org/10.1175/MWR-D-15-0242.1.

Bluestein, H. B., J. C. Snyder, and J. B. Houser, 2015: A multiscale overview of the El Reno, Oklahoma, tornadic supercell of 31 May 2013. *Wea. Forecasting*, **30**, 525–552, https://doi.org/10.1175/WAF-D-14-00152.1.

Brotzge, J., and W. Donner, 2013: The tornado warning process. *Bull. Amer. Meteor. Soc.*, **94**, 1715–1733, https://doi.org/10.1175/BAMS-D-12-00147.1.

Burgess, D. W., R. J. Donaldson Jr., and P. R. Desrochers, 1993: Tornado detection and warning by radar. *The Tornado: Its Structure, Dynamics, Prediction, and Hazards, Geophys. Monogr.*, No. 79, Amer. Geophys. Union, 203–221.

Carlin, J. T., J. Gao, J. C. Snyder, and A. V. Ryzhkov, 2017: Assimilation of Z_{DR} columns for improving the spinup and forecast of convective storms in storm-scale models: Proof-of-concept experiments. *Mon. Wea. Rev.*, **145**, 5033–5057, https://doi.org/10.1175/MWR-D-17-0103.1.

Crum, T. D., S. D. Smith, J. N. Chrisman, R. E. Saffle, R. W. Hall, and R. J. Vogt, 2013: WSR-88D radar projects—Update 2013.

29th Conf. on Environmental Information Processing Technologies, Austin, TX, Amer. Meteor. Soc., 6B.1, https://ams.confex.com/ams/93Annual/webprogram/Paper221461.html.

Deierling, W., and W. A. Peterson, 2008: Total lightning activity as an indicator of updraft characteristics. *J. Geophys. Res.*, **113**, D16210, https://doi.org/10.1029/2007JD009598.

Foote, G. B., 1984: A study of hail growth utilizing observed storm conditions. *J. Climate Appl. Meteor.*, **23**, 84–101, https://doi.org/10.1175/1520-0450(1984)023<0084:ASOHGU>2.0.CO;2.

Forsyth, D. E., and Coauthors, 2005: The National Weather Radar Testbed (phased array). Preprints, *32nd Conf. on Radar Meteorology*, Albuquerque, NM, Amer. Meteor. Soc., 12R.3, https://ams.confex.com/ams/32Rad11Meso/techprogram/paper_96377.htm.

Heinselman, P. L., D. L. Priegnitz, K. L. Manross, T. M. Smith, and R. W. Adams, 2008: Rapid sampling of severe storms by the National Weather Radar Testbed Phased Array Radar. *Wea. Forecasting*, **23**, 808–824, https://doi.org/10.1175/2008WAF2007071.1.

——, D. S. LaDue, and H. Lazrus, 2012: Exploring impacts of rapid-scan radar data on NWS warning decisions. *Wea. Forecasting*, **27**, 1031–1044, https://doi.org/10.1175/WAF-D-11-00145.1.

——, ——, D. M. Kingfield, and R. Hoffman, 2015: Tornado warning decisions using phased array radar data. *Wea. Forecasting*, **30**, 57–78, https://doi.org/10.1175/WAF-D-14-00042.1.

Jung, Y., M. Xue, G. Zhang, and J. M. Straka, 2008: Assimilation of simulated polarimetric radar data for a convective storm using the ensemble Kalman filter. Part II: Impact of polarimetric data on storm analysis. *Mon. Wea. Rev.*, **136**, 2246–2260, https://doi.org/10.1175/2007MWR2288.1.

Knight, C. A., 2006: Very early formation of big, liquid drops revealed by Z_{DR} in continental cumulus. *J. Atmos. Sci.*, **63**, 1939–1953, https://doi.org/10.1175/JAS3721.1.

Kumjian, M. R., 2013: Principles and applications of dual-polarization weather radar. Part II: Warm and cold season applications. *J. Oper. Meteor.*, **1**, 243–264, https://doi.org/10.15191/nwajom.2013.0120.

——, and A. V. Ryzhkov, 2008: Polarimetric signatures in supercell thunderstorms. *J. Appl. Meteor. Climatol.*, **47**, 1940–1961, https://doi.org/10.1175/2007JAMC1874.1.

——, A. P. Khain, N. Benmoshe, E. Ilotoviz, A. V. Ryzhkov, and V. T. J. Phillips, 2014: The anatomy and physics of Z_{DR} columns: Investigating a polarimetric radar signature with a spectral bin microphysical model. *J. Appl. Meteor. Climatol.*, **53**, 1820–1843, https://doi.org/10.1175/JAMC-D-13-0354.1.

Lakshmanan, V., T. Smoth, G. J. Stumpf, and K. Hondl, 2007: The Warning Decision Support System-Integrated Information. *Wea. Forecasting*, **22**, 596–612, https://doi.org/10.1175/WAF1009.1.

——, K. D. Hondl, and R. Rabin, 2009: An efficient, general-purpose technique for identifying storm cells in geospatial images. *J. Atmos. Oceanic Technol.*, **26**, 523–537, https://doi.org/10.1175/2008JTECHA1153.1.

Lemon, L. R., 1998: The radar "three-body scatter spike": An operational large-hail signature. *Wea. Forecasting*, **13**, 327–340, https://doi.org/10.1175/1520-0434(1998)013<0327:TRTBSS>2.0.CO;2.

——, D. W. Burgess, and R. A. Brown, 1978: Tornadic storm airflow and morphology derived from single-Doppler radar measurements. *Mon. Wea. Rev.*, **106**, 48–61, https://doi.org/10.1175/1520-0493(1978)106<0048:TSAAMD>2.0.CO;2.

Lindley, T., and G. Morgan, 2004: The Pecos County, Texas hail storms of 10 May 2002: A null tornado event from a warning decision perspective. *Electron. J. Oper. Meteor.*, **5** (1), http://nwafiles.nwas.org/ej/pdf/2004-EJ1.pdf.

Nelson, S. P., 1983: The influence of storm inflow structure on hail growth. *J. Atmos. Sci.*, **40**, 1965–1983, https://doi.org/10.1175/1520-0469(1983)040<1965:TIOSFS>2.0.CO;2.

NOAA, 2013: Dual-polarization radar: Stepping stones to building a Weather-Ready Nation. NOAA, accessed 1 May 2018, https://www.weather.gov/news/130425-dualpol.

Picca, J. C., and A. V. Ryzhkov, 2010: Z_{DR} columns as a predictive tool for hail growth and storm evaluation. *25th Conf. on Severe Local Storms*, Denver, CO, Amer Meteor. Soc., 11.3, https://ams.confex.com/ams/25SLS/webprogram/Paper175750.html.

——, and ——, 2012: A dual-wavelength polarimetric analysis of the 16 May 2010 Oklahoma City extreme hailstorm. *Mon. Wea. Rev.*, **140**, 1385–1403, https://doi.org/10.1175/MWR-D-11-00112.1.

——, J. C. Snyder, and A. V. Ryzhkov, 2015: An observational analysis of Z_{DR} column trends in tornadic supercells. *37th Conf. on Radar Meteorology*, Norman, OK, Amer. Meteor. Soc., 5A.5, https://ams.confex.com/ams/37RADAR/webprogram/Paper275416.html.

Ryzhkov, A. V., V. B. Zhuravlyov, and N. A. Rybakova, 1994: Preliminary results of X-band polarization radar studies of clouds and precipitation. *J. Atmos. Oceanic Technol.*, **11**, 132–139, https://doi.org/10.1175/1520-0426(1994)011<0132:PROXBP>2.0.CO;2.

Smith, B. T., R. L. Thompson, A. R. Dean, and P. T. Marsh, 2015: Diagnosing the conditional probability of tornado damage rating using environmental and radar attributes. *Wea. Forecasting*, **30**, 914–932, https://doi.org/10.1175/WAF-D-14-00122.1.

Snyder, J. C., A. V. Ryzhkov, M. R. Kumjian, A. P. Khain, and J. C. Picca, 2015: A Z_{DR} column detection algorithm to examine convective storm updrafts. *Wea. Forecasting*, **30**, 1819–1844, https://doi.org/10.1175/WAF-D-15-0068.1.

Supinie, T. A., N. Yussouf, Y. Jung, M. Xue, J. Cheng, and S. Wang, 2017: Comparison of the analysis and forecasts of a tornadic supercell storm from assimilating phased-array radar and WSR-88D observations. *Wea. Forecasting*, **32**, 1379–1401, https://doi.org/10.1175/WAF-D-16-0159.1.

Trapp, R. J., and D. M. Wheatley, 2006: Buyer beware: Some words of caution on the use of severe wind reports in postevent assessment and research. *Wea. Forecasting*, **21**, 408–415, https://doi.org/10.1175/WAF925.1.

Tuttle, J. D., V. N. Bringi, H. D. Orville, and F. J. Kopp, 1989: Multiparameter radar study of a microburst: Comparison with model results. *J. Atmos. Sci.*, **46**, 601–620, https://doi.org/10.1175/1520-0469(1989)046<0601:MRSOAM>2.0.CO;2.

Van Den Broeke, M. S., 2017: Polarimetric radar metrics related to tornado life cycles and intensity in supercell storms. *Mon. Wea. Rev.*, **145**, 3671–3686, https://doi.org/10.1175/MWR-D-16-0453.1.

——, J. M. Straka, and E. N. Rasmussen, 2008: Polarimetric radar observations at low levels during tornado life cycles in a small sample of classic southern plains supercells. *J. Appl. Meteor. Climatol.*, **47**, 1232–1247, https://doi.org/10.1175/2007JAMC1714.1.

WDTD, 2019: Supercell velocity signatures. WDTD, accessed 2 April 2019, https://training.weather.gov/wdtd/courses/rac/severe/supercell-v/presentation_html5.html.

Wicker, L. J., and R. B. Wilhelmson, 1995: Simulation and analysis of tornado development and decay within a three-dimensional supercell thunderstorm. *J. Atmos. Sci.*, **52**, 2675–2703, https://doi.org/10.1175/1520-0469(1995)052<2675:SAAOTD>2.0.CO;2.

Wilson, K. A., P. L. Heinselman, C. M. Kuster, D. M. Kingfield, and Z. Kang, 2017: Forecaster performance and workload: Does radar update time matter? *Wea. Forecasting*, **32**, 253–274, https://doi.org/10.1175/WAF-D-16-0157.1.

Witt, A., M. D. Eilts, G. J. Stumpf, J. T. Johnson, E. D. Mitchell, and K. W. Thomas, 1998: An enhanced hail detection algorithm for the WSR-88D. *Wea. Forecasting*, **13**, 286–303, https://doi.org/10.1175/1520-0434(1998)013<0286:AEHDAF>2.0.CO;2.

Zrnić, D. S., and Coauthors, 2007: Agile-beam phased array radar for weather observations. *Bull. Amer. Meteor. Soc.*, **88**, 1753–1766, https://doi.org/10.1175/BAMS-88-11-1753.